Impact of Phosphorylation on the Physiological Form of Human alpha-Synuclein in Aqueous Solution

Emile de Bruyn,[†,‡,¶] Anton Emil Dorn,[†,‡,§] Giulia Rossetti,[*,‡,‖,⊥] Claudio Fernandez,[#,@] Tiago F. Outeiro,[△,∇,††] Jörg B. Schulz,[¶,⊥,‡‡] and Paolo Carloni[¶,‖]

† *Equally contributed to this work*
‡ *Jülich Supercomputing Centre (JSC), Forschungszentrum Jülich GmbH, 52425 Jülich, Germany*
¶ *Department of Physics, RWTH Aachen University, 52062 Aachen, Germany*
§ *Faculty of Biology, University of Duisburg-Essen, 45141 Essen, Germany*
‖ *Computational Biomedicine (IAS-5/INM-9), Forschungszentrum Jülich GmbH, 52425 Jülich, Germany*
⊥ *Department of Neurology, RWTH Aachen University, 52074 Aachen, Germany*
\# *Max Planck Laboratory for Structural Biology, Chemistry and Molecular Biophysics of Rosario (MPLbioR, UNR-MPINAT). Partner of the Max Planck Institute for Multidisciplinary Sciences (MPINAT, MPG). Centro de Estudios Interdisciplinarios, Universidad Nacional de Rosario, S2002LRK Rosario, Argentina*
@ *Department of NMR-based Structural Biology, Max Planck Institute for Multidisciplinary Sciences, 37077 Göttingen, Germany*
△ *Department of Experimental Neurodegeneration, Center for Biostructural Imaging of Neurodegeneration, University Medical Center Göttingen, 37075 Göttingen, Germany*
∇ *Max Planck Institute for Multidisciplinary Sciences, 37075 Göttingen, Germany*
†† *Translational and Clinical Research Institute, Newcastle University, Newcastle upon Tyne NE1 7RU, United Kingdom*
‡‡ *JARA Brain Institute Molecular Neuroscience and Neuroimaging (INM-11), Research Centre Jülich and RWTH Aachen University, 52074 Aachen, Germany*

E-mail: g.rossetti@fz-juelich.de

Abstract

Serine 129 can be phosphorylated in pathological inclusions formed by the intrinsically disordered protein human α-synuclein (AS), a key player in Parkinson's disease and other synucleinopathies. Here, molecular simulations provide insight into the structural ensemble of phosphorylated AS. The simulations suggest that phosphorylation does not impact the structural content of the physiological AS conformational

ensemble in aqueous solution, as the phosphate group is mostly solvated. The hydrophobic region of AS contains β-hairpin structures, which may increase the propensity of the protein to undergo amyloid formation, as seen in the non-physiological (non-acetylated) form of the protein in a recent molecular simulation study. Our findings are consistent with existing experimental data, with the caveat of the observed limitations of the force field for the phosphorylated moiety.

Introduction

Parkinsons disease (PD) is the second most common neurodegenerative disease after Alzheimer's disease,[1] affecting several million people worldwide.[2,3] The typical pathological hallmark is the accumulation of fibrillar protein inclusions, know as Lewy bodies (LBs) and Lewy neurites (LNs) in the brain.[4,5] The major component of LBs and LNs are fibrillar forms of the human α-synuclein (AS) protein.[3,6] AS is a 140 amino acid 'disordered' conformational ensemble both in aqueous solution and in vivo. AS acquires some degree of structure when bound to the membrane or to cellular partners.[7,8]

The primary sequence of AS can be divided in three domains: the positively charged N-terminus (residues 1-60), the overall neutral hydrophobic region (residues 61-95)[1] and the negatively charged C-terminal domain (residues 96-140, Figure 1). Under physiological conditions, the protein is acetylated on the first residue[2] In LBs, a significant fraction of AS is phosphorylated on S129.[3 11] S129 phosphorylation may be regulated by neuronal activity, suggesting that the process may be part of the normal physiology of AS.[12,13] This post-translational modification (PTM) might play also a pathological role.[14–17] S129 phosphorylation may be regulated by neuronal activity, suggesting that the process may be part of the normal physiology of AS.[12,13]

[1] We choose to use the more accurate term "hydrophobic region" instead of the historical but inaccurate term "non-amyloid component (NAC)".[9]

[2] N-terminal acetylation does not significantly change the fibrillization propensity in vitro.[10]

[3] A novel phosphorylation site of α-synuclein at T64 has also been recently described.[10]

```
MDVFMKGLSKAKEGVVAAAEKTKQGVAEAAGKTKE  35
GVLYVGSKTKEGVVHGVATVAEKTKEQVTNVGGAV  70
VTGVTAVAQKTVEGAGSIAAATGFVKKDQLGKNEE 105
GAPQEGILEDMPVDPDNEAYEMPSEEGYQDYEPEA 140
```

Figure 1: Sequence of amino acid residues in AS; positively charged residues are highlighted in blue and negatively charged ones in red. Three domains can be identified: the positively charged N-terminus (residues 1-60), the overall neutral hydrophobic region (residues 61-95) and the negatively charged C-terminal domain (residues 96-104). In physiological conditions, the protein is acetylated on the first residue, although this post-translational modification does not significantly affect the fibrillization propensity in vitro.[18] In LBs, a significant fraction of AS is phosphorylated on S129.[11] A novel phosphorylation site at T64 has also been recently described.[10]

The formation of the S129-O-PO_3^{2-} group at the C-terminus of phosphorylated α synuclein (pAS) instead of one of the other two domains is intriguing, because it introduces as many as two negative charges at physiological pH (the pKa_1 and pKa_2 of phosphoserine are < 2 and 5.6[19]).[4]

The impact of phosphorylation on the structural ensemble and aggregation propensity of physiological AS is not known. Thus far, Circular Dichroisim (CD) studies on the non-N-term acetylated form of the protein show that the conformational ensemble does not change significantly upon S129 phosphorylation in solution.[20,21] [5] On the detailed molecular level, replica exchange simulations based on the CHARMM36m force field[23] point to an increase of looped secondary structure close to a β-hairpin spread throughout the hydrophobic region upon phosphorylation.[24] However, the structure of the physiological form differs from that of the non-acetylated one (which does not exist in human cells),[25–27] so firm conclusions on the effect of phosphorylation on endogenous AS cannot be made from these studies.

Here we investigate the impact of phosphorylation on AS' physiological form by molecular simulation. For this study, one may face several challenges. First, the force field must be adequate to describe IDPs such as AS. The DES-Amber ff99SB,[28] the Amber a99SB-

[4]It might be possible that the phosphate is partially monoprotonated. The effect of protonation is discussed in the Supplementary Information.

[5]This contrasts with findings by CD studies for phosphorylation on protein variants.[20–22] These point to significant changes in the structural ensemble upon phosphorylation.

disp[29] and CHARMM36m[23] force fields have been tailored for IDPs[29–31] and the last two have already been successfully used for the non-acetylated form of the proteins.[29,31,32] All of these force fields appear therefore to be well suited to study AS. Second, accurately describing a doubly charged group such as phosphate in pAS is non-trivial. Parameters for phosphorylated serine, threonine, and tyrosine for the Amber[33–35] and CHARMM[36,37] force fields have been published. Those for the DES-Amber force field have been recently calibrated on osmotic coefficient calculations.[38] Unfortunately, simulation studies based on such parametrizations have at times shown artifacts.[39–42] In addition, none of them describe the hydration properties of the phosphate moiety.[39–47] This may be very important to fully establish the accuracy of the parametrization. Finally, the conformational space of the protein structural ensemble needs to be efficiently explored. Among the many methodologies used to investigate IDPs successfully,[48–57] our predictions based on Replica Exchange with Solute Tempering 2 (REST2)[58] enhanced sampling predictions of wild-type[59,60] and mutants of AS,[60,61] turned out to reproduce a variety of biophysical properties of the protein and hence they appear well suitable to study this problem.

Here, we present REST2 simulations of AS and pAS based on the DES-Amber[38] and a99SB-*disp* force-fields.[29] We use TIP4P-D for DES-Amber, and the accompanying modified TIP4P-D water model for a99SB-*disp*. To the best of the authors' knowledge, these simulations are the only ones so far (i) reporting on the physiological form of AS in explicit solvent,[6] and (ii) describing in detail the hydration properties of the phosphate.

[6]Many molecular simulation studies, besides those in refs. 29,32, focus on the non-acetylated protein.[31,62–64,64–85] Calculations of the protein in implicit solvent are not reported here.

Methods

Molecular Simulations

The initial structure of the acetylated protein (AS) which best reproduced the chemical shifts in ref. 86 was selected from the conformational ensemble previously reported in ref. 59. The phosphorylated protein (pAS) was built by adding a phosphate group to S129 using PyMOL.[87]

AS and pAS were inserted in a water-filled dodecahedral simulation box with periodic boundary conditions and minimum distance of 35 Å between the protein and the box edges. Na^+ and Cl^- ions were added to neutralize the system and achieve a concentration of 150 mmol L^{-1}. Table 1 shows the composition of the systems.

Table 1: Number of atoms in the simulation box for the three systems simulated here.

	Protein	Water	Sodium	Chlorine
AS	2,020	190,533	186	176
pAS	2,023	172,359	171	159

The simulations were based on: (i) the DES-Amber force field[28] and the standard TIP4P-D water model[88] (Table S1 for a full list of the parameters used); (ii) the a99SB-*disp* force field[29] and its accompanying modified TIP4P-D water model.[29] Long range electrostatics were evaluated using the Particle-Mesh Ewald (PME) method,[89] using a cutoff distance of 12 Å in real space. The van der Waals interactions featured the same cutoff.

Constant temperature conditions were achieved by coupling the systems with a Nosé-Hoover thermostat[90] at 300 K, with a time constant of 0.5 ps. Constant pressure was achieved with a Parrinello-Rahman barostat[91] at 1 bar, with a time constant of 2 ps (Table S1). The LINCS algorithm was used for all bonds involving hydrogen atoms.[92] The equations of motions were integrated using the `md` leap-frog algorithm, with a timestep of 2 fs.

The proteins underwent energy minimization (Table S2), and, subsequently 100 ps of MD in the NVT ensemble (Table S3). Then, they were heated up in 25 ps-long steps of 5 K in

the same ensemble up to 300 K using simulated annealing (Tables S4 and S5). The systems were further equilibrated for 1 ns in the NPT ensemble (Table S6). Finally, they underwent 100 ns REST2 simulations[58] in the NPT ensemble. The proteins were not found to be near their periodic images at distances lower than 12 Å during any of these simulations. The simulations converged after 12 ns (see the Results Section).

Structurally similar conformational clusters were obtained following the method for clustering IDPs described in ref. 93: For both AS and pAS, a total of 8.000 frames from the converged trajectories were clustered (Figures S1 and S2).

The following properties were calculated for conformations after convergence: (i) The radius of gyration R_g, calculated using the MDTraj Python code.[94] (ii) The hydrodynamic radius, calculated from the radii of gyration using the linear fit of ref. 72. (iii) The NMR chemical shifts of the C_α atoms, calculated using the shiftx2 code.[95] (iv) The CD spectra, using the DichroCalc code.[96] Additionally the average of all conformational clusters, weighted to their occurrence along the trajectory, was calculated. (v) The solvent accessible surface area (SASA) using the MDTraj code.[94] (vi) The contact map of protein residues using minimum pairwise distances between residues using the MDTraj code.[94] (vii) Radial distribution functions (RDFs) from the oxygen atoms of S129 using the SPEADI[97,98] code developed by the authors.

Hydrogen bonds were defined according to the scheme in ref. 99. These were identified using the MDTraj code.[94] (ix) Salt bridges were defined using a distance between two charged atoms in the protein at a distance below 3.25 Å as in ref. 100. The MDTraj code[94] was also used to identify these. Secondary structure elements were identified using MDTraj[94] and DSSP.[101]

Results and Discussion

We performed REST2 simulations[58] for 100 ns, using 32 replicas, for both AS and pAS in aqueous solution. The calculations were based on the DES-Amber[38] and the a99SB-*disp* force fields,[29] both already used for IDPs. We report results at length for calculations using the former, while we provide a summary for the latter here and details in the Supplementary Information.

Convergence. We calculated two quantities as a function of simulated time to investigate the convergence of the systems (Figures S3 to S6): (i) the running averages of the percentage of secondary structures. In particular, helix structures reached a plateau after 12 ns; (ii) the running averages of the C_α chemical shifts which converge closely to the experimental values within 12 ns. Because of the limitations of the standard usage of RMSD with IDPs such as AS,[102] the running RMSD of atomic positions was not taken into account. Based on this analysis, we calculated structural properties in the interval 12–100 ns.

Comparison with experiment. The computational setup results in trajectories that reproduce the experimental data (NMR, CD and hydrodynamic radius)[21,27,86] available for AS (Figures S5 to S7 and Table S8).

Effect of phosphorylation. The ten most frequent conformational clusters of AS and pAS represent a total of 47.7 % and 52.9 % of the converged simulation trajectories, respectively (Table S7). They are presented in Figures 2 and 3.

The mean calculated hydrodynamic radii agree with the experimental values (28.2 and 35.3 Å for AS and pAS,[22] respectively), within the standard deviation (Table 2). These and the mean radii of gyration (R_g) decrease slightly upon phosphorylation (still within the margin of error, Table 2). The distribution of R_g, however, differs significantly between AS and pAS (Figure 4(a)): the latter displays a higher propensity for either compact or extended conformations than AS. At the qualitative level, this changes the free energy landscape of the protein to form two slightly deeper basins instead of a more shallow landscape (Figures 4(b) and 4(c)). Interestingly, pAS displays a higher likelihood to retain a compact conformation,

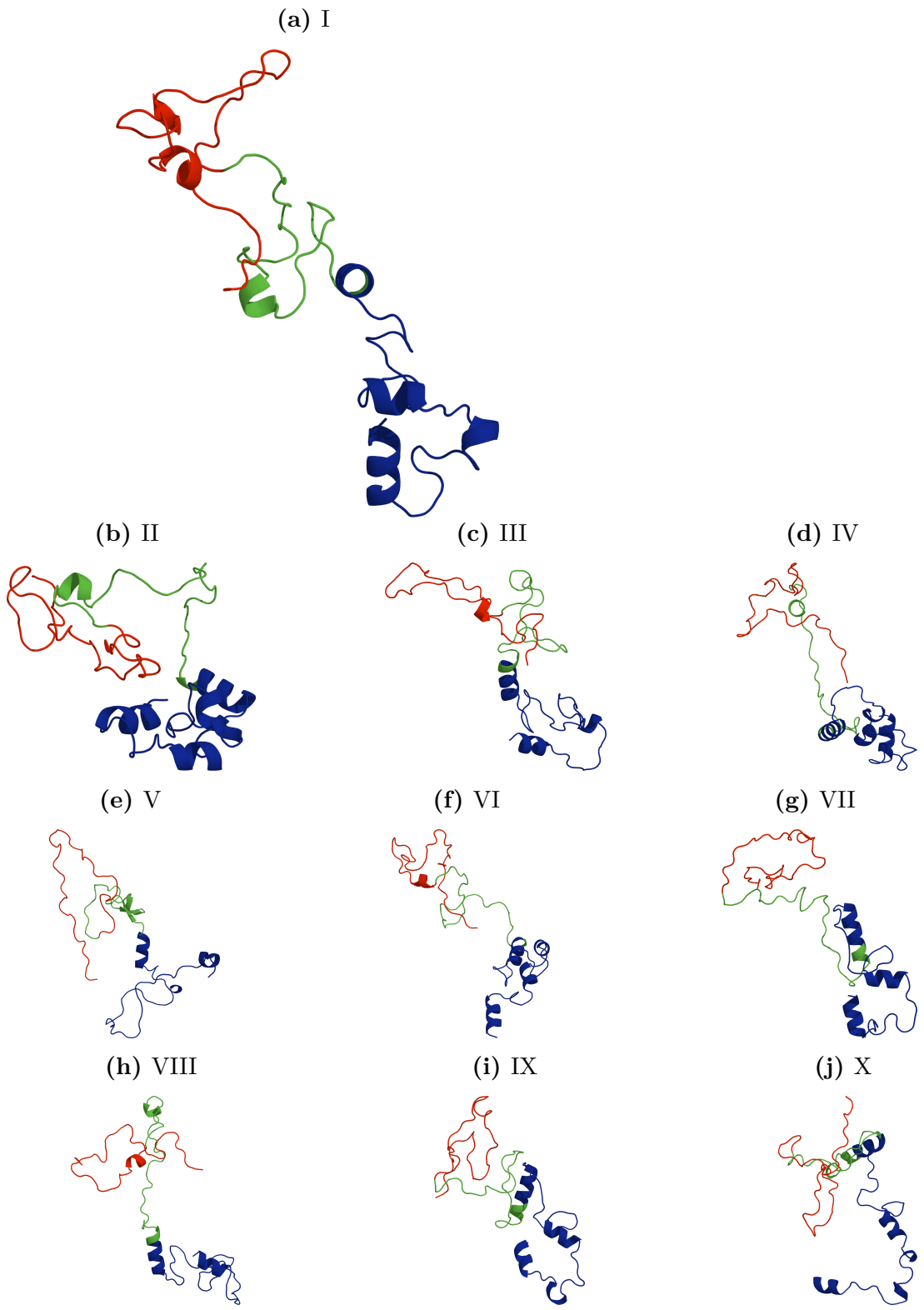

Figure 2: Representative structures (I-X) of AS as determined by clustering. The N-terminal domain is colored blue, the hydrophobic region green and the C-terminal domain red. The percentage of occurrence of the structures decreases from left to right and top to bottom (Table S7).

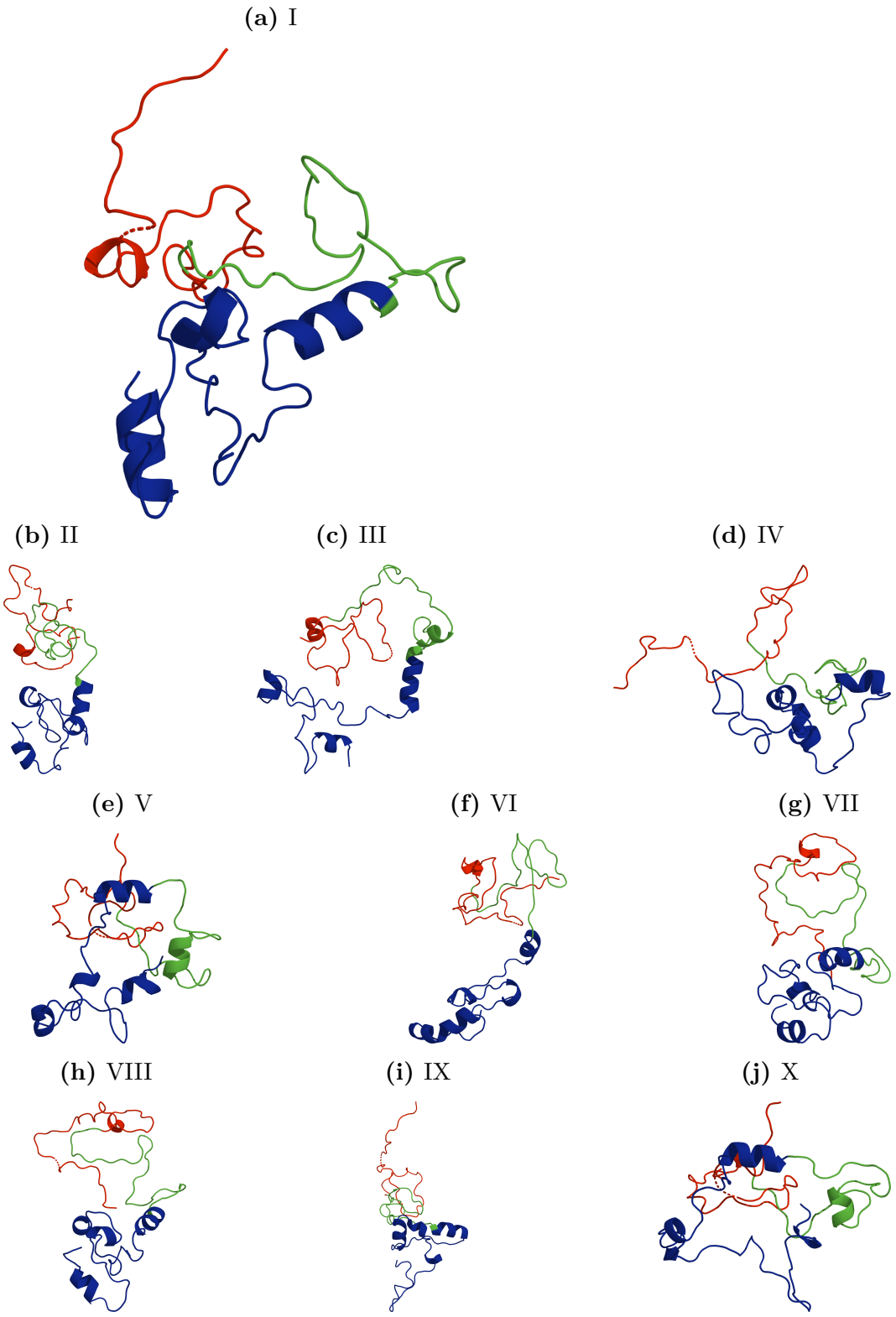

Figure 3: Representative structures (I-X) of pAS as determined by clustering. The acetyl group at the N-terminus and the residue at position S129 are shown as ball and sticks. The percentage of occurrence of the structures decreases from left to right and top to bottom (Table S7).

even when the distance between the termini increases.

Table 2: Calculated properties of AS and pAS. (i) Hydrodynamic R_H and gyration (R_g) radii of the entire proteins and of the hydrophobic regions (HR). (ii) Average number of hydrogen bonds. (iii) Average number of salt bridges. Standard deviations are indicated in parenthesis.

Protein	R_H [Å]	R_g [Å]	R_g(HR) [Å]	R_H(HR) [Å]	N_{SB}	N_{HB}
AS	35.1 (± 6.1)	35.6 (± 12.8)	23.8 (± 16.4)	28.3 (± 11.3)	1.54 (± 1.23)	19.52 (± 4.28)
pAS	31.0 (± 5.8)	28.0 (± 9.6)	17.2 (± 9.2)	23.1 (± 8.1)	1.86 (± 1.75)	20.67 (± 4.32)

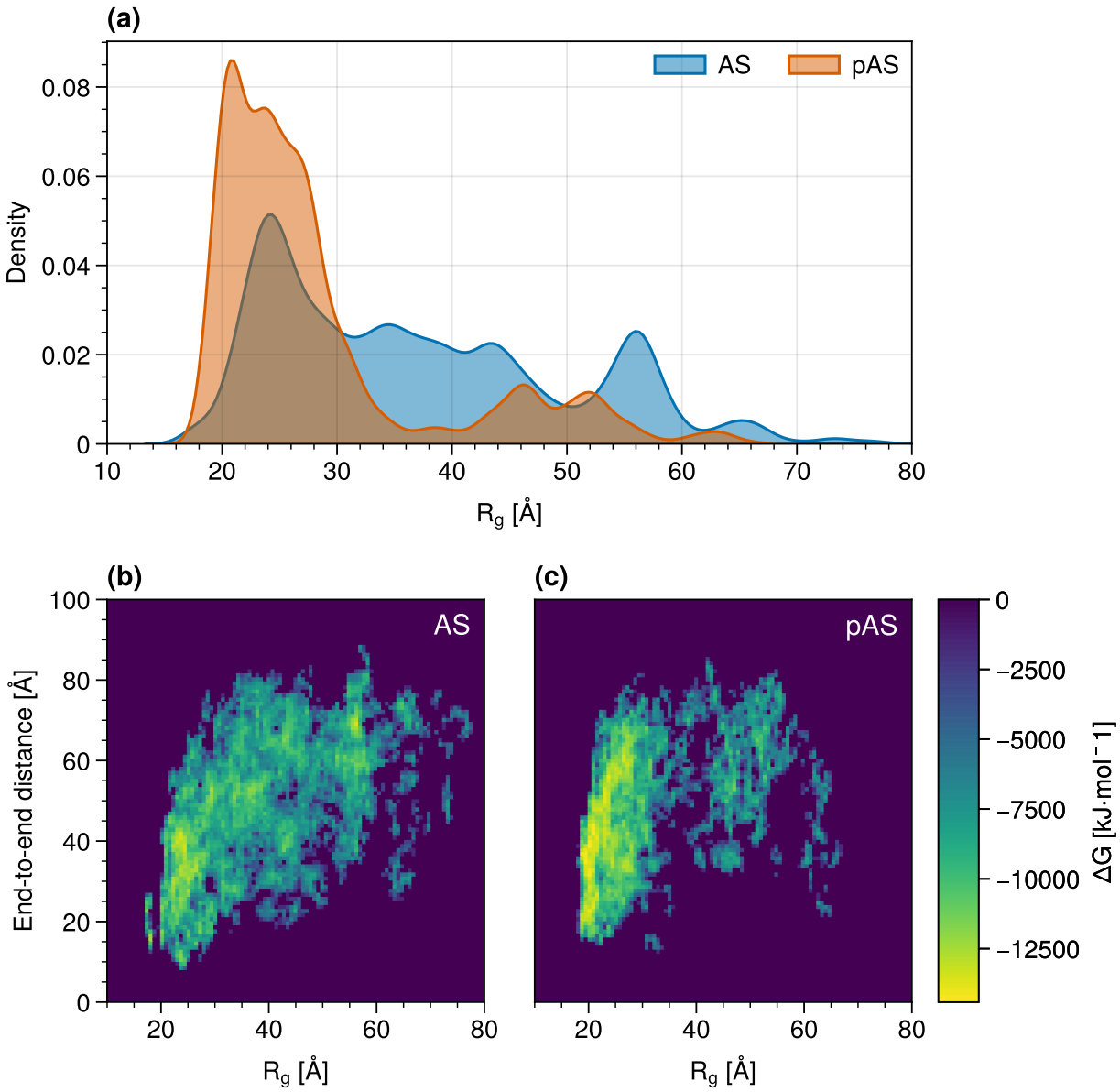

Figure 4: R_g distribution for AS (blue) and pAS (orange) (a) and the corresponding (highly approximate) free energy landscapes plotted as a function of the distance between the protein termini (b-c).

The solvent accessibility increases in the hydrophobic region (Table 3). However, because of the large fluctuations of the C-terminus – N-terminus distances (Figure S8), this analysis is not conclusive.

The intramolecular interactions between the hydrophobic region and the other regions slightly increase upon phosphorylation, as shown by the contact maps for each monomer

and their differences (Figure 5). Accordingly, the number of intramolecular hydrogen bonds increases (6(a-b)). However, the results should be taken with caution, as the number of such interactions shows a wide normal distribution with a large standard deviation (Table 2).

Table 3: Average Solvent Accessible Surface Area (SASA) in AS and pAS in the hydrophobic region (HR) and at the N- and C-termini.

Protein	$SASA_N$ [Å^2]	$SASA_{HR}$ [Å^2]	$SASA_C$ [Å^2]
AS	96 (± 41)	87 (± 31)	111 (± 32)
pAS	90 (± 42)	91 (± 32)	113 (± 39)

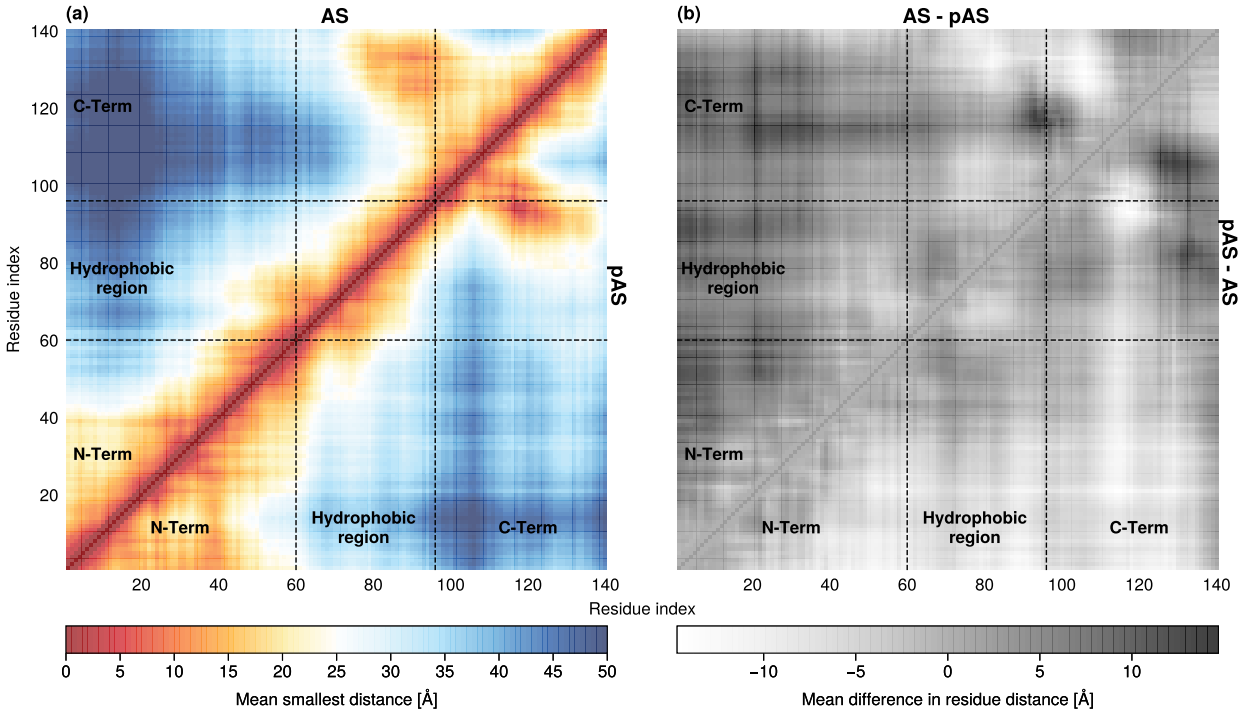

Figure 5: (a) Contact maps of AS (triangle above) and pAS (triangle below). (b) Mean residue distance differences between AS (triangle above) and pAS (triangle below). Brighter corresponds to comparatively closer distances.

These H-bonds are almost exclusively formed within every single domain (Figures 6(a-b)).

The number of salt bridges increases upon phosphorylation. The most persistent salt bridges common to both forms involve the N-term and hydrophobic regions (K23–E20 and K58–E61, respectively, see Figures 6(a-b)). Few salt bridges are formed between the C-terminus and one of the two other domains. Of course, because the intramolecular contacts

of IDPs are labile, the scenario could be different over longer time scales or at different starting points.

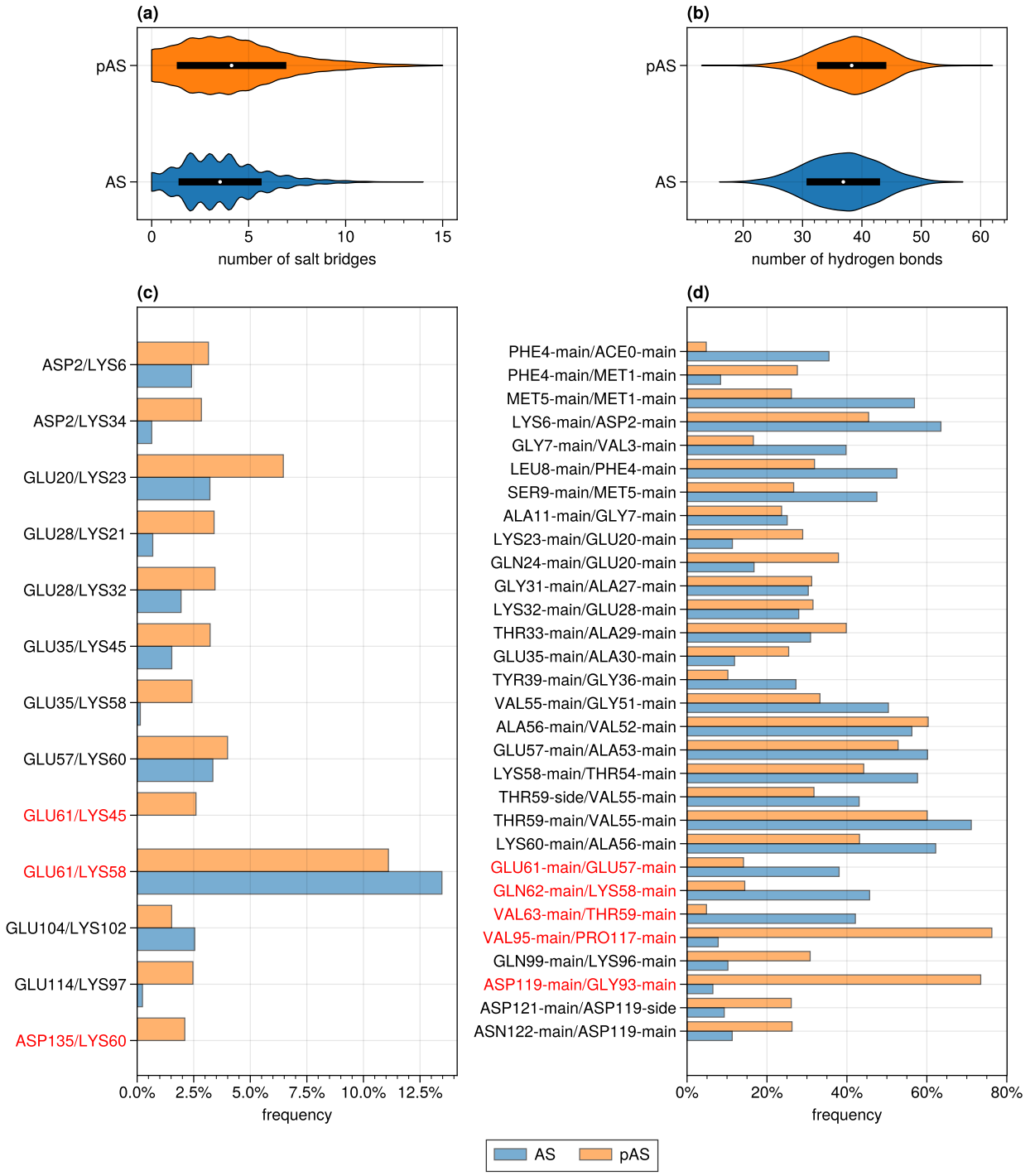

Figure 6: Distribution of the total number of salt bridges (a) and hydrogen bonds (b) in AS (blue) and pAS (orange). Frequency with which intradomain (black labels) and interdomain (red labels) salt bridges (a) and hydrogen bonds (b) are found in AS and pAS. Shown are salt bridges and hydrogen bonds that occur during at least 2 % and 25 % of the converged trajectory, respectively, in either the AS or pAS simulation.

We conclude that the protein's conformational ensemble becomes *slightly* more compact upon phosphorylation. This is associated with a small increase of intramolecular interactions. This is expected, as the increase of negative charge at the C-terminus can increase its interaction with the rest of the protein, and particularly with the positively charged N-terminus: the phosphate group interacts to a small extent with sodium ions (Figure S17) and, even less, with the protein residues (Figure S16). In fact, this group is fully solvent exposed, as shown by a plot of the phosphate oxygen-water oxygen RDFs (Figure 7). This may be caused, at least in part, by the presence of four negatively charged phosphate oxygen atoms.[7] Within these caveats, we suggest that the electrostatic field of the phosphate is strongly reduced by its solvation and does not impact the C-terminus-N-terminus interactions. This lack of interaction may also in part be explained by AS containing no arginine residues that are known to interact strongly with phosphate groups,[103] and indeed none of the lysine residues present in the N-terminal domain formed salt bridges with S129 during the simulation (Figure 6).

In AS, S129 interacts much less with the solvent than phosphate in pAS: The Oγ atom has only 2 water hydrogen (Figure 7) and no sodium ions in its surrounding. The serine oxydril group instead forms a variety of *intramolecular* H-bonds (with K80, K96, K97, K102, E126, E130 and E131 (Figure S16). S129 backbone units are observed to interact both with the solvent and nearby protein hydrogens in both AS and pAS. Thus, S129 forms many more intermolecular contacts than the phosphorylated residue in pAS.

[7]The phosphate oxygen charges in the CHARMM[36,37] and Amber[34] parametrizations, also used to study phopshate PTMs in IDPs, are not too dissimilar to those of used here ($-0.565$to-0.639 e). In the case of Amber-based simulations of pAS, reported in the Supplementary Information, we also see an overestimation of interacting water molecules.

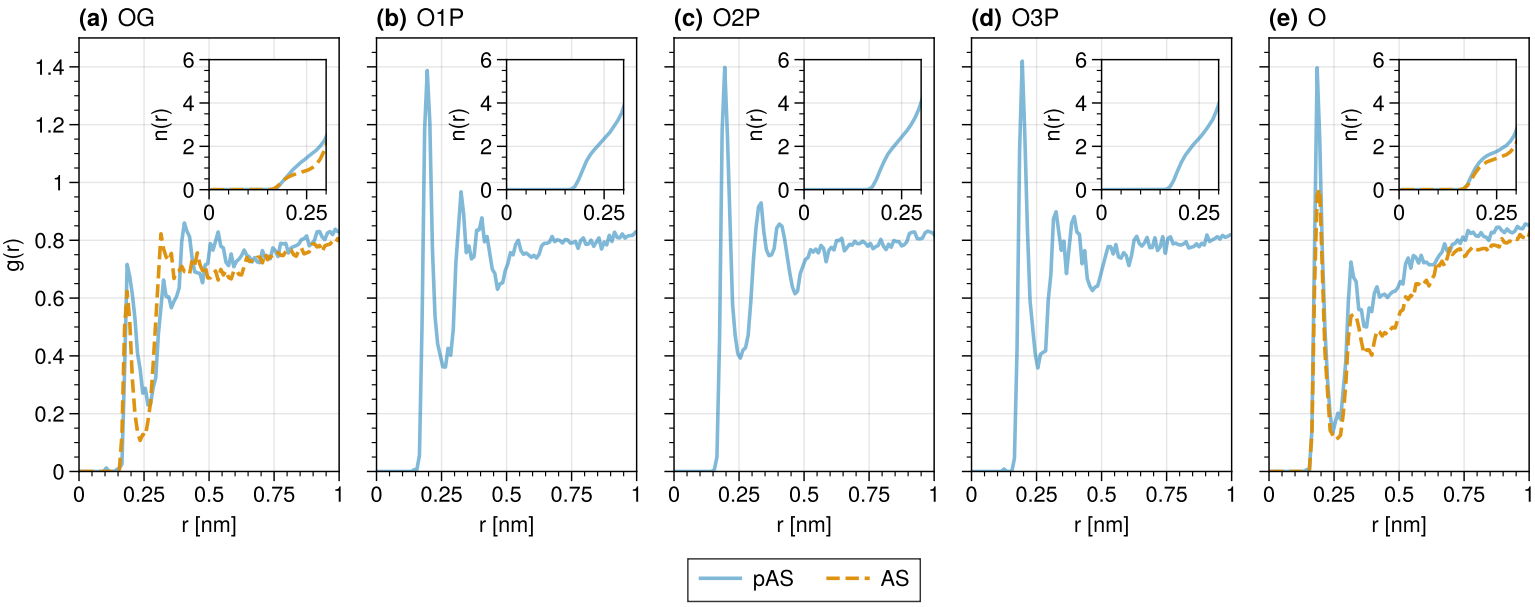

Figure 7: RDFs ($g(r)$) of the oxygen atoms of residue 129 and water hydrogens (a-e). Compare the RDF for pAS (blue) and AS (orange) for the oxygen atom in the side chain (a) and the carbonyl oxygen (e). (b-d) illustrate the RDF for the terminal phosphoryl oxygens. Insets show the integral of $g(r)$ up to 0.3 nm.

Using the approach of ref. 24, we find a significant content of β-hairpin-like structure in the hydrophobic region upon phosphorylation (Figure S20).[8] As discussed in ref. 24, these types of structures may be associated with amyloid-forming conformations and hence this finding does suggest that phosphorylation increases fibril formation starting from conformations similar to those found in the fibrils.[104,105] This would be consistent with the fact that almost all the proteins in the fibrils are phosphorylated *in vivo*.[11]

These simulation results show overall only a small change in the structural ensemble of aqueous physiological AS upon phosphorylation at S129. Our previously published simulations of familial-PD linked mutations of AS[98] display far greater changes in the structural ensemble relative to the wild-type, compared to phosphorylation in the current study. The simulations here are in line with experimental studies showing that phosphorylation and de-phosphorylation of AS are likely normal physiological processes fine-tuning binding to

[8]This content is however smaller than that observed for the non-physiological form, see details in the Supplementary Information

lipids,[106,107] not a clear marker of pathology.[12,13] This, however, does not preclude the prevailing view that phosphorylation is also implicated in fibril formation.[12]

The simulations of AS and pAS with the Amber a99SB-*disp* force field[29] show very similar results as those presented here, except for the phosphate hydration properties, which turn out to be less accurate than those of the DES-Amber force field (See Supplemementary Information, Sections 4, 5).

The simulations of the protein with monoprotonated phosphate (based on the a99SB-*disp* force field) turn out to be rather similar to those of pAS (see Supplementary Information, Section 6). Thus, we conclude that if such species exist in equilibrium with pAS, they contribute to the protein structural ensemble similarly to pAS.

Conclusions

Because of the presence *in vivo* of phosphorylated AS, the detailed understanding of the impact of phosphorylation on this protein is important for informing therapeutic strategies aimed at targeting AS in synucleinopathies. Here, we investigated the effects of phosphorylation on the structural ensemble of AS in solution by REST2 simulations. Our simulations of AS are consistent with a plethora of experimental data, as in our previous simulations.[59] Most importantly, our study of the as yet unexplored physiological form of pAS concludes that it also does not undergo large conformational changes relative to the physiological form of AS. The small changes are consistent with CD studies of phosphorylation on the non-physiological form of AS.[20,21] The protein simply becomes slightly more compact than the unmodified protein. As seen for the non-physiological form of the protein 24, phosphorylation induces a β-hairpin-like, amyloid-forming conformations. The increased propensity towards fibril formation is likely consistent with the fact that about 90 % AS in the LBs is phosphorylated.[11]

Supporting Information Available

The data that support the findings of this study are available from the corresponding author, GR, upon reasonable request.

Detailed experimental setup, analysis and comparison with results obtained with other force fields are contained in the Supplementary Information (PDF).

Structures of the 30 most frequently found cluster midpoints are included for both AS and pAS (PDB).

Acknowledgement

TFO is supported by DFG (SFB1286-B8) and under Germanys Excellence Strategy - EXC 2067/1- 390729940.

This work was partially performed as part of the Helmholtz School for Data Science in Life, Earth and Energy (HDS-LEE) and received funding from the Helmholtz Association of German Research Centers.

Open Access publication funded by the Deutsche Forschungsgemeinschaft (DFG, German Research Foundation) 491111487.

The authors gratefully acknowledge the Gauss Centre for Supercomputing e.V. (www.gauss-centre.eu) for funding this project by providing computing time through the John von Neumann Institute for Computing (NIC) on the GCS Supercomputer JUWELS at Jülich Supercomputing Centre (JSC).[108–111]

The authors gratefully acknowledge insightful discussions with Stefano Piana-Agostinetti regarding the choice of force field parameters, in particular with respect to the hydration of the phosphate group.

References

(1) Hou, Y.; Dan, X.; Babbar, M.; Wei, Y.; Hasselbalch, S. G.; Croteau, D. L.; Bohr, V. A. Ageing as a risk factor for neurodegenerative disease. *Nature Reviews Neurology* **2019**, *15*, 565–581.

(2) Rocca, W. A. The burden of Parkinson's disease: a worldwide perspective. *The Lancet* **2018**, *17*, 928–929.

(3) Lücking, C. B.; Brice, A. Alpha-synuclein and Parkinson's disease. *Cellular and Molecular Life Sciences CMLS* **2000**, *57*, 18941908.

(4) Baba, M.; Nakajo, S.; Tu, P.-H.; Tomita, T.; Nakaya, K.; Lee, V.; Trojanowski, J. Q.; Iwatsubo, T. Aggregation of alpha-synuclein in Lewy bodies of sporadic Parkinson's disease and dementia with Lewy bodies. *The American journal of pathology* **1998**, *152*, 879–884.

(5) Gibb, W.; Lees, A. The relevance of the Lewy body to the pathogenesis of idiopathic Parkinson's disease. *Journal of Neurology, Neurosurgery & Psychiatry* **1988**, *51*, 745–752.

(6) Nguyen, P. H.; Ramamoorthy, A.; Sahoo, B. R.; Zheng, J.; Faller, P.; Straub, J. E.; Dominguez, L.; Shea, J.-E.; Dokholyan, N. V.; De Simone, A., *et al.* Amyloid oligomers: A joint experimental/computational perspective on Alzheimers disease, Parkinsons disease, type II diabetes, and amyotrophic lateral sclerosis. *Chemical reviews* **2021**, *121*, 2545–2647.

(7) Snead, D.; Eliezer, D. Alpha-synuclein function and dysfunction on cellular membranes. *Experimental neurobiology* **2014**, *23*, 292.

(8) Waudby, C. A.; Camilloni, C.; Fitzpatrick, A. W.; Cabrita, L. D.; Dobson, C. M.; Vendruscolo, M.; Christodoulou, J. In-cell NMR characterization of the secondary

structure populations of a disordered conformation of α-synuclein within E. coli cells. *PloS one* **2013**, *8*, e72286.

(9) Goedert, M.; Griesinger, C.; Outeiro, T. F.; Riek, R.; Schröder, G. F.; Spillantini, M. G. Abandon the Nac in α-synuclein. *The Lancet Neurology* **2024**, *23*, 669.

(10) Matsui, H.; Ito, S.; Matsui, H.; Ito, J.; Gabdulkhaev, R.; Hirose, M.; Yamanaka, T.; Koyama, A.; Kato, T.; Tanaka, M., *et al.* Phosphorylation of α-synuclein at T64 results in distinct oligomers and exerts toxicity in models of Parkinsons disease. *Proceedings of the National Academy of Sciences* **2023**, *120*, e2214652120.

(11) Fujiwara, H.; Hasegawa, M.; Dohmae, N.; Kawashima, A.; Masliah, E.; Goldberg, M. S.; Shen, J.; Takio, K.; Iwatsubo, T. α-Synuclein Is Phosphorylated in Synucleinopathy Lesions. *Nature Cell Biology* **2002**, *4*, 160–164.

(12) Ramalingam, N. *et al.* Dynamic Physiological α-synuclein S129 Phosphorylation Is Driven By Neuronal Activity. *npj Parkinson's Disease* **2023**, *9*, 4.

(13) Ramalingam, N.; Haass, C.; Dettmer, U. Physiological Roles of α-synuclein Serine-129 Phosphorylation - Not an Oxymoron. *Trends in Neurosciences* **2024**, *nil*, nil.

(14) Ghanem, S. S.; Majbour, N. K.; Vaikath, N. N.; Ardah, M. T.; Erskine, D.; Jensen, N. M.; Fayyad, M.; Sudhakaran, I. P.; Vasili, E.; Melachroinou, K., *et al.* α-Synuclein phosphorylation at serine 129 occurs after initial protein deposition and inhibits seeded fibril formation and toxicity. *Proceedings of the National Academy of Sciences* **2022**, *119*, e2109617119.

(15) Wang, Y.; Shi, M.; Chung, K. A.; Zabetian, C. P.; Leverenz, J. B.; Berg, D.; Srulijes, K.; Trojanowski, J. Q.; Lee, V. M.-Y.; Siderowf, A. D., *et al.* Phosphorylated α-synuclein in Parkinsons disease. *Science translational medicine* **2012**, *4*, 121ra20–121ra20.

(16) Kawahata, I.; Finkelstein, D. I.; Fukunaga, K. Pathogenic Impact of α-Synuclein Phosphorylation and Its Kinases in α-Synucleinopathies. *International Journal of Molecular Sciences* **2022**, *23*, 6216.

(17) Oueslati, A.; Fournier, M.; Lashuel, H. A. Role of post-translational modifications in modulating the structure, function and toxicity of α-synuclein: implications for Parkinsons disease pathogenesis and therapies. *Progress in brain research* **2010**, *183*, 115–145.

(18) Fauvet, B.; Fares, M.-B.; Samuel, F.; Dikiy, I.; Tandon, A.; Eliezer, D.; Lashuel, H. A. Characterization of Semisynthetic and Naturally Nα-Acetylated α-Synuclein in Vitro and in Intact Cells. *Journal of Biological Chemistry* **2012**, *287*, 28243–28262.

(19) Xie, Y.; Jiang, Y.; Ben-Amotz, D. Detection of amino acid and peptide phosphate protonation using Raman spectroscopy. *Analytical biochemistry* **2005**, *343*, 223–230.

(20) Schreurs, S.; Gerard, M.; Derua, R.; Waelkens, E.; Taymans, J.-M.; Baekelandt, V.; Engelborghs, Y. In vitro phosphorylation does not influence the aggregation kinetics of WT α-synuclein in contrast to its phosphorylation mutants. *International journal of molecular sciences* **2014**, *15*, 1040–1067.

(21) Samuel, F.; Flavin, W. P.; Iqbal, S.; Pacelli, C.; Renganathan, S. D. S.; Trudeau, L.-E.; Campbell, E. M.; Fraser, P. E.; Tandon, A. Effects of serine 129 phosphorylation on α-synuclein aggregation, membrane association, and internalization. *Journal of Biological Chemistry* **2016**, *291*, 4374–4385.

(22) Paleologou, K. E.; Schmid, A. W.; Rospigliosi, C. C.; Kim, H.-Y.; Lamberto, G. R.; Fredenburg, R. A.; Lansbury, P. T.; Fernandez, C. O.; Eliezer, D.; Zweckstetter, M., *et al.* Phosphorylation at Ser-129 but not the phosphomimics S129E/D inhibits the fibrillation of α-synuclein. *Journal of Biological Chemistry* **2008**, *283*, 16895–16905.

(23) Huang, J.; Rauscher, S.; Nawrocki, G.; Ran, T.; Feig, M.; de Groot, B. L.; Grubmüller, H.; MacKerell, A. D. Charmm36m: an Improved Force Field for Folded and Intrinsically Disordered Proteins. *Nature Methods* **2016**, *14*, 71–73.

(24) Semenyuk, P. I. Alpha-Synuclein Phosphorylation Induces Amyloid Conversion Via Enhanced Electrostatic Bridging: Insights From Molecular Modeling of the Full-Length Protein. *Biophysical Chemistry* **2024**, *307*, 107196.

(25) Kang, L.; Moriarty, G. M.; Woods, L. A.; Ashcroft, A. E.; Radford, S. E.; Baum, J. N-Terminal Acetylation of α-synuclein Induces Increased Transient Helical Propensity and Decreased Aggregation Rates in the Intrinsically Disordered Monomer. *Protein Science* **2012**, *21*, 911–917.

(26) Trexler, A. J.; Rhoades, E. Nterminal Acetylation Is Critical for Forming αhelical Oligomer of αsynuclein. *Protein Science* **2012**, *21*, 601–605.

(27) Maltsev, A. S.; Ying, J.; Bax, A. Impact of N-terminal acetylation of α-synuclein on its random coil and lipid binding properties. *Biochemistry* **2012**, *51*, 5004–5013.

(28) Piana, S.; Robustelli, P.; Tan, D.; Chen, S.; Shaw, D. E. Development of a force field for the simulation of single-chain proteins and protein–protein complexes. *Journal of chemical theory and computation* **2020**, *16*, 2494–2507.

(29) Robustelli, P.; Piana, S.; Shaw, D. E. Developing a molecular dynamics force field for both folded and disordered protein states. *Proceedings of the National Academy of Sciences* **2018**, *115*, E4758–E4766.

(30) Wang, W. Recent advances in atomic molecular dynamics simulation of intrinsically disordered proteins. *Phys. Chem. Chem. Phys.* **2021**, *23*, 777–784.

(31) Pedersen, K. B.; Flores-Canales, J. C.; Schiøtt, B. Predicting molecular properties of

α-synuclein using force fields for intrinsically disordered proteins. *Proteins: Structure, Function, and Bioinformatics* **2023**, *91*, 47–61.

(32) Robustelli, P.; de Opakua, A. I.; Campbell-Bezat, C.; Giordanetto, F.; Becker, S.; Zweckstetter, M.; Pan, A. C.; Shaw, D. E. Molecular Basis of Small-Molecule Binding To α-Synuclein. *Journal of the American Chemical Society* **2022**, *144*, 2501–2510.

(33) Homeyer, N.; Horn, A. H.; Lanig, H.; Sticht, H. AMBER force-field parameters for phosphorylated amino acids in different protonation states: phosphoserine, phosphothreonine, phosphotyrosine, and phosphohistidine. *Journal of molecular modeling* **2006**, *12*, 281–289.

(34) Steinbrecher, T.; Latzer, J.; Case, D. Revised AMBER parameters for bioorganic phosphates. *Journal of chemical theory and computation* **2012**, *8*, 4405–4412.

(35) Khoury, G. A.; Thompson, J. P.; Smadbeck, J.; Kieslich, C. A.; Floudas, C. A. Forcefield_PTM: Ab initio charge and AMBER forcefield parameters for frequently occurring post-translational modifications. *Journal of chemical theory and computation* **2013**, *9*, 5653–5674.

(36) Petrov, D.; Margreitter, C.; Grandits, M.; Oostenbrink, C.; Zagrovic, B. A systematic framework for molecular dynamics simulations of protein post-translational modifications. *PLoS computational biology* **2013**, *9*, e1003154.

(37) Zhong, B.; Song, G.; Chen, H.-F. Balanced Force Field ff03CMAP Improving the Dynamics Conformation Sampling of Phosphorylation Site. *International Journal of Molecular Sciences* **2022**, *23*, 11285.

(38) Tucker, M. R.; Piana, S.; Tan, D.; LeVine, M. V.; Shaw, D. E. Development of Force Field Parameters for the Simulation of Single- and Double-Stranded Dna Molecules and Dna-Protein Complexes. *The Journal of Physical Chemistry B* **2022**, *126*, 4442–4457.

(39) Vymětal, J.; Jurásková, V.; Vondrášek, J. AMBER and CHARMM force fields inconsistently portray the microscopic details of phosphorylation. *Journal of Chemical Theory and Computation* **2018**, *15*, 665–679.

(40) Rieloff, E.; Skepö, M. Phosphorylation of a disordered peptideStructural effects and force field inconsistencies. *Journal of chemical theory and computation* **2020**, *16*, 1924–1935.

(41) Rieloff, E.; Skepö, M. Molecular Dynamics Simulations of Phosphorylated Intrinsically Disordered Proteins: a Force Field Comparison. *International Journal of Molecular Sciences* **2021**, *22*, 10174.

(42) Man, V. H.; He, X.; Gao, J.; Wang, J. Phosphorylation of Tau R2 Repeat Destabilizes Its Binding to Microtubules: A Molecular Dynamics Simulation Study. *ACS Chemical Neuroscience* **2023**,

(43) Jin, F.; Gräter, F. How Multisite Phosphorylation Impacts the Conformations of Intrinsically Disordered Proteins. *PLOS Computational Biology* **2021**, *17*, e1008939.

(44) Rieloff, E.; Skepö, M. The Effect of Multisite Phosphorylation on the Conformational Properties of Intrinsically Disordered Proteins. *International Journal of Molecular Sciences* **2021**, *22*, 11058.

(45) Martin, I. M.; Aponte-Santamaría, C.; Schmidt, L.; Hedtfeld, M.; Iusupov, A.; Musacchio, A.; Gräter, F. Phosphorylation Tunes Elongation Propensity and Cohesiveness of Incenp's Intrinsically Disordered Region. *Journal of Molecular Biology* **2022**, *434*, 167387.

(46) Adhikari, S.; Mondal, J. Machine Learning Subtle Conformational Change Due To Phosphorylation in Intrinsically Disordered Proteins. *The Journal of Physical Chemistry B* **2023**, *127*, 9433–9449.

(47) Amith, W. D.; Dutagaci, B. Complex Conformational Space of the Rna Polymerase Ii C-Terminal Domain Upon Phosphorylation. *The Journal of Physical Chemistry B* **2023**, *127*, 9223–9235.

(48) Irbäck, A.; Mohanty, S. Profasi: a Monte Carlo Simulation Package for Protein Folding and Aggregation. *Journal of Computational Chemistry* **2006**, *27*, 1548–1555.

(49) D'Urzo, A.; Konijnenberg, A.; Rossetti, G.; Habchi, J.; Li, J.; Carloni, P.; Sobott, F.; Longhi, S.; Grandori, R. Molecular Basis for Structural Heterogeneity of an Intrinsically Disordered Protein Bound To a Partner By Combined Esi-Im-Ms and Modeling. *Journal of The American Society for Mass Spectrometry* **2014**, *26*, 472–481.

(50) Cragnell, C.; Rieloff, E.; Skepö, M. Utilizing Coarse-Grained Modeling and Monte Carlo Simulations To Evaluate the Conformational Ensemble of Intrinsically Disordered Proteins and Regions. *Journal of Molecular Biology* **2018**, *430*, 2478–2492.

(51) Rieloff, E.; Tully, M. D.; Skepö, M. Assessing the Intricate Balance of Intermolecular Interactions Upon Self-Association of Intrinsically Disordered Proteins. *Journal of Molecular Biology* **2019**, *431*, 511–523.

(52) Shrestha, U. R.; Smith, J. C.; Petridis, L. Full Structural Ensembles of Intrinsically Disordered Proteins From Unbiased Molecular Dynamics Simulations. *Communications Biology* **2021**, *4*, 243.

(53) Gupta, A.; Dey, S.; Hicks, A.; Zhou, H.-X. Artificial Intelligence Guided Conformational Mining of Intrinsically Disordered Proteins. *Communications Biology* **2022**, *5*, 610.

(54) Yu, H.; Han, W.; Ma, W.; Schulten, K. Transient β-hairpin Formation in α-synuclein Monomer Revealed By Coarse-Grained Molecular Dynamics Simulation. *The Journal of Chemical Physics* **2015**, *143*, 243142.

(55) Cragnell, C.; Durand, D.; Cabane, B.; Skepö, M. Coarse-Grained Modeling of the Intrinsically Disordered Protein Histatin 5 in Solution: Monte Carlo Simulations in Combination With Saxs. *Proteins: Structure, Function, and Bioinformatics* **2016**, *84*, 777–791.

(56) Hyltegren, K.; Polimeni, M.; Skepö, M.; Lund, M. Integrating All-Atom and Coarse-Grained Simulations-Toward Understanding of Idps At Surfaces. *Journal of Chemical Theory and Computation* **2020**, *16*, 1843–1853.

(57) Garaizar, A.; Espinosa, J. R. Salt Dependent Phase Behavior of Intrinsically Disordered Proteins From a Coarse-Grained Model With Explicit Water and Ions. *The Journal of Chemical Physics* **2021**, *155*, 125103.

(58) Wang, L.; Friesner, R. A.; Berne, B. Replica exchange with solute scaling: a more efficient version of replica exchange with solute tempering (REST2). *The Journal of Physical Chemistry B* **2011**, *115*, 9431–9438.

(59) Rossetti, G.; Musiani, F.; Abad, E.; Dibenedetto, D.; Mouhib, H.; Fernandez, C. O.; Carloni, P. Conformational ensemble of human α-synuclein physiological form predicted by molecular simulations. *Physical Chemistry Chemical Physics* **2016**, *18*, 5702–5706.

(60) Palomino-Hernandez, O.; Buratti, F. A.; Sacco, P. S.; Rossetti, G.; Carloni, P.; Fernandez, C. O. Role of Tyr-39 for the Structural Features of α-Synuclein and for the Interaction with a Strong Modulator of Its Amyloid Assembly. *International journal of molecular sciences* **2020**, *21*, 5061.

(61) Theillet, F.-X.; Binolfi, A.; Bekei, B.; Martorana, A.; Rose, H. M.; Stuiver, M.; Verzini, S.; Lorenz, D.; Van Rossum, M.; Goldfarb, D., *et al.* Structural disorder of monomeric α-synuclein persists in mammalian cells. *Nature* **2016**, *530*, 45–50.

(62) Uluca, B.; Viennet, T.; Petrović, D.; Shaykhalishahi, H.; Weirich, F.; Gönülalan, A.; Strodel, B.; Etzkorn, M.; Hoyer, W.; Heise, H. DNP-enhanced MAS NMR: a tool to snapshot conformational ensembles of α-synuclein in different states. *Biophysical journal* **2018**, *114*, 1614–1623.

(63) Jain, K.; Ghribi, O.; Delhommelle, J. Folding free-energy landscape of α-synuclein (35–97) via replica exchange molecular dynamics. *Journal of Chemical Information and Modeling* **2020**, *61*, 432–443.

(64) Ilie, I. M.; Nayar, D.; Den Otter, W. K.; Van Der Vegt, N. F.; Briels, W. J. Intrinsic conformational preferences and interactions in α-synuclein fibrils: insights from molecular dynamics simulations. *Journal of chemical theory and computation* **2018**, *14*, 3298–3310.

(65) Chwastyk, M.; Cieplak, M. Conformational biases of α-synuclein and formation of transient knots. *The Journal of Physical Chemistry B* **2019**, *124*, 11–19.

(66) Perlmutter, J. D.; Braun, A. R.; Sachs, J. N. Curvature dynamics of α-synuclein familial parkinson disease mutants. *Journal of Biological Chemistry* **2009**, *284*, 7177–7189.

(67) Allison, J. R.; Varnai, P.; Dobson, C. M.; Vendruscolo, M. Determination of the free energy landscape of α-synuclein using spin label nuclear magnetic resonance measurements. *Journal of the American Chemical Society* **2009**, *131*, 18314–18326.

(68) Amos, S.-B. T.; Schwarz, T. C.; Shi, J.; Cossins, B. P.; Baker, T. S.; Taylor, R. J.; Konrat, R.; Sansom, M. S. Membrane Interactions of α-Synuclein Revealed by Multiscale Molecular Dynamics Simulations, Markov State Models, and NMR. *The Journal of Physical Chemistry B* **2021**, *125*, 2929–2941.

(69) Herrera, F. E.; Chesi, A.; Paleologou, K. E.; Schmid, A.; Munoz, A.; Vendruscolo, M.; Gustincich, S.; Lashuel, H. A.; Carloni, P. Inhibition of α-synuclein fibrillization by

dopamine is mediated by interactions with five C-terminal residues and with E83 in the NAC region. *PloS one* **2008**, *3*, e3394.

(70) Robustelli, P.; Ibanez-de Opakua, A.; Campbell-Bezat, C.; Giordanetto, F.; Becker, S.; Zweckstetter, M.; Pan, A. C.; Shaw, D. E. Molecular basis of small-molecule binding to α-synuclein. *Journal of the American Chemical Society* **2022**, *144*, 2501–2510.

(71) Balesh, D.; Ramjan, Z., *et al.* Unfolded annealing molecular dynamics conformers for wild-type and disease-associated variants of alpha-synuclein show no propensity for beta-sheetformation. *Journal of Biophysical Chemistry* **2011**, *2011*.

(72) Allison, J. R.; Rivers, R. C.; Christodoulou, J. C.; Vendruscolo, M.; Dobson, C. M. A relationship between the transient structure in the monomeric state and the aggregation propensities of α-synuclein and β-synuclein. *Biochemistry* **2014**, *53*, 7170–7183.

(73) Dedmon, M. M.; Lindorff-Larsen, K.; Christodoulou, J.; Vendruscolo, M.; Dobson, C. M. Mapping long-range interactions in α-synuclein using spin-label NMR and ensemble molecular dynamics simulations. *Journal of the American Chemical Society* **2005**, *127*, 476–477.

(74) Park, S.; Yoon, J.; Jang, S.; Lee, K.; Shin, S. The role of the acidic domain of α-synuclein in amyloid fibril formation: a molecular dynamics study. *Journal of Biomolecular Structure and Dynamics* **2016**, *34*, 376–383.

(75) Brodie, N. I.; Popov, K. I.; Petrotchenko, E. V.; Dokholyan, N. V.; Borchers, C. H. Conformational ensemble of native α-synuclein in solution as determined by short-distance crosslinking constraint-guided discrete molecular dynamics simulations. *PLoS computational biology* **2019**, *15*, e1006859.

(76) Tsigelny, I. F.; Bar-On, P.; Sharikov, Y.; Crews, L.; Hashimoto, M.; Miller, M. A.; Keller, S. H.; Platoshyn, O.; Yuan, J. X.-J.; Masliah, E. Dynamics of α-synuclein ag-

gregation and inhibition of pore-like oligomer development by β-synuclein. *The FEBS journal* **2007**, *274*, 1862–1877.

(77) Ramis, R.; Ortega-Castro, J.; Casasnovas, R.; Mariño, L.; Vilanova, B.; Adrover, M.; Frau, J. A coarse-grained molecular dynamics approach to the study of the intrinsically disordered protein α-synuclein. *Journal of chemical information and modeling* **2019**, *59*, 1458–1471.

(78) Yu, H.; Han, W.; Ma, W.; Schulten, K. Transient β-hairpin formation in α-synuclein monomer revealed by coarse-grained molecular dynamics simulation. *The Journal of chemical physics* **2015**, *143*, 12B623_1.

(79) Narayanan, C.; Weinstock, D. S.; Wu, K.-P.; Baum, J.; Levy, R. M. Investigation of the polymeric properties of α-synuclein and comparison with NMR experiments: a replica exchange molecular dynamics study. *Journal of chemical theory and computation* **2012**, *8*, 3929–3942.

(80) Dibenedetto, D.; Rossetti, G.; Caliandro, R.; Carloni, P. A molecular dynamics simulation-based interpretation of nuclear magnetic resonance multidimensional heteronuclear spectra of α-synuclein $\cdot$ dopamine adducts. *Biochemistry* **2013**, *52*, 6672–6683.

(81) Tsigelny, I. F.; Sharikov, Y.; Miller, M. A.; Masliah, E. Mechanism of alpha-synuclein oligomerization and membrane interaction: theoretical approach to unstructured proteins studies. *Nanomedicine: Nanotechnology, Biology and Medicine* **2008**, *4*, 350–357.

(82) Zhang, T.; Tian, Y.; Li, Z.; Liu, S.; Hu, X.; Yang, Z.; Ling, X.; Liu, S.; Zhang, J. Molecular dynamics study to investigate the dimeric structure of the full-length α-synuclein in aqueous solution. *Journal of Chemical Information and Modeling* **2017**, *57*, 2281–2293.

(83) Savva, L.; Platts, J. A. How Cu (II) binding affects structure and dynamics of α-synuclein revealed by molecular dynamics simulations. *Journal of Inorganic Biochemistry* **2023**, *239*, 112068.

(84) Razzokov, J.; Fazliev, S.; Makhkamov, M.; Marimuthu, P.; Baev, A.; Kurganov, E. Effect of Electric Field on α-Synuclein Fibrils: Revealed by Molecular Dynamics Simulations. *International Journal of Molecular Sciences* **2023**, *24*, 6312.

(85) Savva, L.; Platts, J. A. Exploring the Impact of Mutation and Post-Translational Modification on α-Synuclein: Insights From Molecular Dynamics Simulations With and Without Copper. *Journal of Inorganic Biochemistry* **2023**, *249*, 112395.

(86) Roche, J.; Ying, J.; Maltsev, A. S.; Bax, A. Impact of Hydrostatic Pressure on an Intrinsically Disordered Protein: A High-Pressure NMR Study of α-Synuclein. *ChemBioChem* **2013**, *14*, 1754–1761.

(87) DeLano, W. L., *et al.* Pymol: An open-source molecular graphics tool. *CCP4 Newsletter on protein crystallography* **2002**, *40*, 82–92.

(88) Piana, S.; Donchev, A. G.; Robustelli, P.; Shaw, D. E. Water Dispersion Interactions Strongly Influence Simulated Structural Properties of Disordered Protein States. *The Journal of Physical Chemistry B* **2015**, *119*, 5113–5123.

(89) Darden, T.; York, D.; Pedersen, L. Particle mesh Ewald: An N log (N) method for Ewald sums in large systems. *The Journal of chemical physics* **1993**, *98*, 10089–10092.

(90) Evans, D. J.; Holian, B. L. The nose–hoover thermostat. *The Journal of chemical physics* **1985**, *83*, 4069–4074.

(91) Andersen, H. C. Molecular dynamics simulations at constant pressure and/or temperature. *The Journal of chemical physics* **1980**, *72*, 2384–2393.

(92) Hess, B.; Bekker, H.; Berendsen, H. J.; Fraaije, J. G. LINCS: a linear constraint solver for molecular simulations. *Journal of computational chemistry* **1997**, *18*, 1463–1472.

(93) Appadurai, R.; Koneru, J. K.; Bonomi, M.; Robustelli, P.; Srivastava, A. Clustering Heterogeneous Conformational Ensembles of Intrinsically Disordered Proteins With T-Distributed Stochastic Neighbor Embedding. *Journal of Chemical Theory and Computation* **2023**, *19*, 4711–4727.

(94) McGibbon, R. T.; Beauchamp, K. A.; Harrigan, M. P.; Klein, C.; Swails, J. M.; Hernández, C. X.; Schwantes, C. R.; Wang, L.-P.; Lane, T. J.; Pande, V. S. MDTraj: A Modern Open Library for the Analysis of Molecular Dynamics Trajectories. *Biophysical Journal* **2015**, *109*, 1528 – 1532.

(95) Han, B.; Liu, Y.; Ginzinger, S. W.; Wishart, D. S. SHIFTX2: significantly improved protein chemical shift prediction. *Journal of biomolecular NMR* **2011**, *50*, 43–57.

(96) Bulheller, B. M.; Hirst, J. D. DichroCalccircular and linear dichroism online. *Bioinformatics* **2009**, *25*, 539–540.

(97) de Bruyn, E. SPEADI: Scalable Protein Environment Analysis for Dynamics and Ions (v1.0.0). 2022; `https://doi.org/10.5281/zenodo.7436713`.

(98) de Bruyn, E.; Dorn, A. E.; Zimmermann, O.; Rossetti, G. Speadi: Accelerated Analysis of Idp-Ion Interactions From MD-Trajectories. *Biology* **2023**, *12*, 581.

(99) Wernet, P.; Nordlund, D.; Bergmann, U.; Cavalleri, M.; Odelius, M.; Ogasawara, H.; Näslund, L. A.; Hirsch, T. K.; Ojamäe, L.; Glatzel, P.; Pettersson, L. G. M.; Nilsson, A. The Structure of the First Coordination Shell in Liquid Water. *Science* **2004**, *304*, 995–999.

(100) Donald, J. E.; Kulp, D. W.; DeGrado, W. F. Salt Bridges: Geometrically Specific,

Designable Interactions. *Proteins: Structure, Function, and Bioinformatics* **2011**, *79*, 898–915.

(101) Kabsch, W.; Sander, C. Dictionary of protein secondary structure: pattern recognition of hydrogen-bonded and geometrical features. *Biopolymers: Original Research on Biomolecules* **1983**, *22*, 2577–2637.

(102) Lazar, T.; Guharoy, M.; Vranken, W.; Rauscher, S.; Wodak, S. J.; Tompa, P. Distance-Based metrics for comparing conformational ensembles of intrinsically disordered proteins. *Biophysical Journal* **2020**, *118*, 2952–2965.

(103) Mandel-Gutfreund, Y.; Schueler, O.; Margalit, H. Comprehensive Analysis of Hydrogen Bonds in Regulatory Protein Dna-Complexes: in Search of Common Principles. *Journal of Molecular Biology* **1995**, *253*, 370–382.

(104) Guerrero-Ferreira, R.; Taylor, N. M.; Mona, D.; Ringler, P.; Lauer, M. E.; Riek, R.; Britschgi, M.; Stahlberg, H. Cryo-Em Structure of Alpha-Synuclein Fibrils. *eLife* **2018**, *7*, nil.

(105) Guerrero-Ferreira, R. *et al.* Two New Polymorphic Structures of Human Full-Length Alpha-Synuclein Fibrils Solved By Cryo-Electron Microscopy. *eLife* **2019**, *8*, nil.

(106) Bell, R.; Vendruscolo, M. Modulation of the Interactions Between α-Synuclein and Lipid Membranes By Post-Translational Modifications. *Frontiers in Neurology* **2021**, *12*, nil.

(107) Killinger, B. A.; Mercado, G.; Choi, S.; Tittle, T.; Chu, Y.; Brundin, P.; Kordower, J. H. Distribution of Phosphorylated Alpha-Synuclein in Non-Diseased Brain Implicates Olfactory Bulb Mitral Cells in Synucleinopathy Pathogenesis. *npj Parkinson's Disease* **2023**, *9*, 43.

(108) Krause, D. Juwels: Modular Tier-0/1 Supercomputer At Jülich Supercomputing Centre. *Journal of large-scale research facilities JLSRF* **2019**, *5*, A135.

(109) Alvarez, D. Juwels Cluster and Booster: Exascale Pathfinder With Modular Supercomputing Architecture At Juelich Supercomputing Centre. *Journal of large-scale research facilities JLSRF* **2021**, *7*, A183.

(110) Herten, A. JUWELS Booster - Early User Experiences. Proceedings of the 2021 on Performance EngineeRing, Modelling, Analysis, and VisualizatiOn STrategy. 2021; p nil.

(111) Kesselheim, S. *et al. Lecture Notes in Computer Science*; Lecture Notes in Computer Science; Springer International Publishing, 2021; pp 453–468.

TOC Graphic

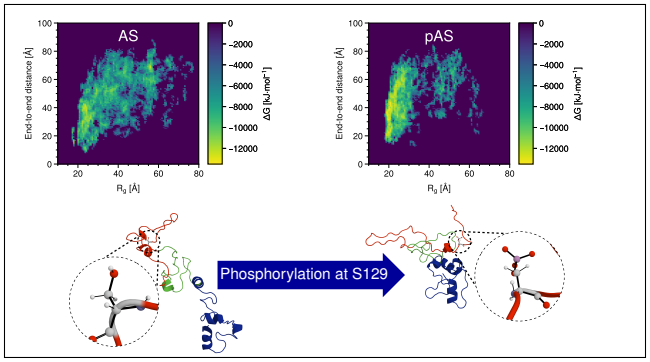
AS
pAS
End-to-end distance [Å]
R_g [Å]
ΔG [kJ·mol^{-1}]
Phosphorylation at S129